Energy Proceedings
Vol 39, 2024
ISSN 2004-2965

Multi-Period Optimization of Hydrogen-Based Steelmaking System: A Rolling-Horizon Approach

Kangling Sheng[1], Xiaojun Wang[1,2], Fangyuan Si[1,2*], Zhao Liu[1,2], Yizhi Zhang[1], Jinghan He[1,2]

1 School of Electrical Engineering, Beijing Jiaotong University, Beijing 100044, China

2 Beijing Engineering Research Center of Electric Rail Transportation, Beijing 100044, China
(*Corresponding Author: fysi@bjtu.edu.cn)

ABSTRACT

Under the "Dual-Carbon" targets, hydrogen production powered by renewable energy and hydrogen direct reduction offer approaches to integrating a high proportion of renewable energy and catalyzing the steel industry's transition towards a low-carbon footprint. The hydrogen-based steelmaking system (HBSS) presents a multi-energy interaction, encompassing processes from hydrogen production and ironmaking to the final steelmaking processes. Additionally, the high investment and operational expenses necessitate that decision-makers prioritize enhancing the system's economic efficiency to ensure its long-term viability and effectiveness. In this study, we first introduced a multi-period optimization model for HBSS, aiming to reduce the levelized cost of steel (LCOS) from both the investment and operational aspects. Then, the rolling-horizon approach has been used to overcome computational infeasibility for large mixed-integer linear programming problems by solving the problem periodically, including additional information from proximately following periods. We further compared it with the single-period and forward-looking approaches, indicating that the optimal result of LCOS varied from $406 to $520 for the different approaches. It proves that the rolling-horizon approach can lead to an economics-better solution than the single-period approach and is only a few percent away from the forward-looking approach.

Keywords: multi-period optimization, rolling-horizon approach, industrial decarbonization, hydrogen-based steelmaking, renewable energy resources, energy transition

NONMENCLATURE

Abbreviations	
H_2	Hydrogen
H_2-SF	Hydrogen Direct Reduction Shaft Furnace
EAF	Electric Arc Furnace
DRI	Direct Reduction Iron
HBI	Hot-Briquetted Iron
TSP	Total Steel Production
CO_2	Carbon Dioxide
TOU	Time of Use
RESs	Renewable Energy Sources
CUC	Clustered Unit Commitment
HBSS	Hydrogen-Based Steelmaking System
LCOS	Levelized Cost of Steel
H_2-DRI	Hydrogen-Based Direct Reduction

1. INTRODUCTION

1.1 Motivation

Accelerating the transition to green and low-carbon energy has become a global consensus and collective action. The global community has established a series of timelines and goals in response to carbon neutrality. On the one hand, this considers the issue of emission pollution, and on the other hand, it considers the finiteness of fossil fuels. Unlike fossil fuels, RESs such as WT and PV can provide a sustainable energy guarantee for humanity. According to the International Energy Agency (IEA), renewables' share of the power generation mix worldwide is set to rise from 29% to 35% by 2025. However, the growth of renewable power generation and integration into the grid presents a challenge to the

This is a paper for 15th International Conference on Applied Energy (ICAE2023), Dec. 3-7, 2023, Doha, Qatar.

absorption of renewable energy with random fluctuations [1], [2].

Meanwhile, steel is a vital commodity for all modern economies. The steel industry, however, is notably energy- and emission-intensive, which has a significant environmental impact [3]. As the world's largest energy consumer among industrial sectors, the steel industry has witnessed a rising trend in production in recent years. According to statistics from the World Steel Association, in 2020, a total of 1.86 billion tons of steel was produced worldwide, with the steel industry's direct carbon emissions amounting to approximately 3.5 billion tons, accounting for 7% to 9% of global carbon emissions from human activities. China's annual crude steel output grew from 129 Mt in 2000 to 1.064 Bt in 2020, marking an increase of about 7.3 times.

1.2 Literature review

Focusing on the decarbonization target of the steel industry [4], a more promising application of hydrogen is acting as a reducing agent in the production of H_2-DRI [5], [6]. With the improvement of both the hydrogen supply system [7]–[9] and the H_2-based direct reduction [10]–[12], H_2-based steelmaking has promoted a fossil fuel-free pathway for the steel industry [13]–[15]. By integrating high-energy-consuming industries with RESs, it hopes to absorb more RESs and effectively reduce industrial carbon emissions [16]. Steel manufacturers have launched several notable projects to investigate the commercial feasibility of hydrogen-based steelmaking processe [17]–[19]. Meanwhile, as scrap steel is a recycled resource, increasing the scrap ratio in the steelmaking process can decrease raw material costs [20] and advance more energy-efficient production.

Research focused on the optimization of HBSS is primarily aimed at achieving a specific objective, such as minimizing overall system costs or emissions, which is pursued through three interrelated research strands:

The first strand of research centered on the design of multi-energy flows within the systems, as highlighted in studies [21], [22]. It further extends to examining the influence of various uncertainties on the optimal operation of the system. Factors such as fluctuations in electricity prices, carbon costs, and equipment prices are critically analyzed in the study [23].

The second strand shifts focus on evaluating the techno-economic feasibility on a system level, which involves an analysis that integrates technical performance with economic viability, assessing the financial aspects of hydrogen utilization to produce steel along the proposed route [24], [25].

The third strand is dedicated to assessing the potential for decarbonization potential [26]–[29], which adopts a socio-technical perspective to examine the full industrial processes, therefore, extends the discussion from the specificities of HBSS design and feasibility to the broader implications for environmental sustainability.

Building upon the following research, most research considers the so-called single-period approach in their investment decision-making, which considers a singular investment period followed by multiple operational periods. Typical parameters, which are assumed to be known within the considered time horizon since these are readily available, are used in this approach. However, parameters, such as demand and prices, are updated in the coming future, considering the investment scheme of the system at different stages in the future from the perspective of multi-period planning is conducive to achieving better source-load matching and improving the economy of long-time frame investment [30].

Multi-period optimization models are typically constructed by setting objective functions and constraints to identify investments and operational decisions over the life cycle, such as operating, investment, and emission costs [31], [32]. When the decision horizon achieves a long time frame, the multi-optimized model will include a large number of variables and constraints, which can be too complex to be solved in a reasonable time. The choice of foresight or the decision horizon can significantly impact the efficiency of solving optimization problems.

Fig.1 illustrates the different decision horizon alternatives of single-period, forward-looking [32], and rolling-horizon [33] approaches for solving multi-period optimization problems over a large period. As for the forward-looking approach, investment decisions are made with full knowledge of the lifetime. In contrast, as for the rolling-horizon approach, investment decisions are made sequentially.

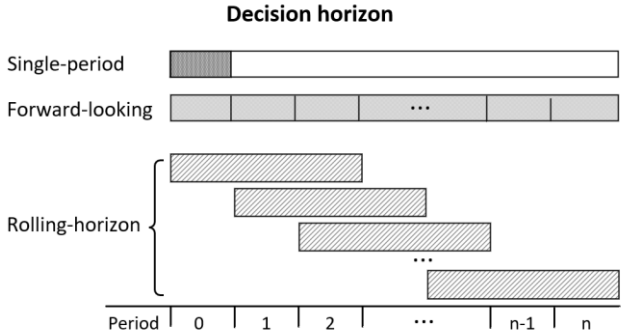

Fig. 1. Decision horizon alternatives of single-period, forward-looking, and rolling-horizon approaches.

1.3 Contribution

The major contributions of our work are threefold:

Firstly, we address a model of HBSS encompassing each piece of energy equipment that allows us to delve into the intricate interrelationships of multi-energy flows within HBSS.

Further, we employ a weekly resolution in our model, which can capture the operational characteristics of HBSS, including the combination of daily, weekly, and seasonal dynamics, and provide a framework for analyzing the efficiency and effectiveness of HBSS in various scenarios.

Finally, we develop a multi-period optimization model for HBSS to minimize LCOS across the lifecycle, ensuring its long-term economic and operational efficiency. Then, we compared the optimization results and computational efficiency under different approaches.

1.4 Paper organization

The remaining parts are structured as follows: Section 2 presents the structure of a hydrogen-based steelmaking system. The optimization framework for solving the multi-period optimization problem using the rolling-horizon approach is shown in Section 3. Case study and result analysis are performed in Section 4. Conclusions are given in Section 5.

2. DESCRIPTION OF HBSS

2.1 Schematic of the energy flow of HBSS

The hydrogen-based steelmaking system is a multi-energy coupled system that integrates various energy technologies such as PEM electrolyzer, H_2 storage, H_2-SF, HBI storage, and EAF, WT, PV, and the power grid provide the electricity supplied to the system for the electrolyzer, hydrogen direct reduction shaft furnace, and electric arc furnace.

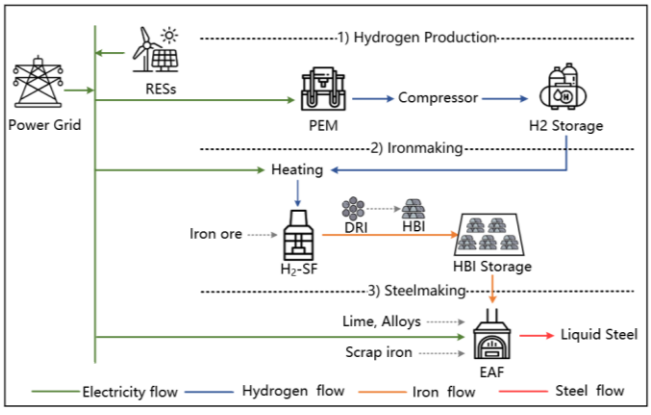

Fig.2. Schematic of the energy flow of HBSS

Fig.2 illustrates the schematic of the energy flow of HBSS, which can be divided into three steps: hydrogen production, ironmaking and steelmaking.

2.2 CUC model of PEM electrolyzer

PEM electrolyzer possesses the highest operational flexibility and turndown capability and has a low minimum load, short start-time, and high ramp rate. The operating characteristics of the PEM electrolyzer can be determined as:

$$\begin{cases} \mu_{\text{E.min}} S_{\text{E}.k} \le P_{\text{E}}^{t} \le \mu_{\text{E.max}} S_{\text{E}.k} \\ \left| P_{\text{E}.k}^{t} - P_{\text{E}.k}^{t-1} \right| \le \Delta P_{\text{E.max}} \end{cases} \tag{1}$$

$$G_{\text{E}.k}^{t} = P_{\text{E}.k}^{t} / \lambda_{\text{E}.k} \tag{2}$$

$$\begin{cases} s_{\text{E}.k}^{t-\alpha} - d_{\text{E}.k}^{t} = u_{\text{E}.k}^{t} - u_{\text{E}.k}^{t-1} \\ u_{\text{E}.k}^{1} = u_{\text{E}.k}^{T} \\ s_{\text{E}.k}^{t} \le 1 - s_{\text{E}.k}^{t-1} \\ d_{\text{E}.k}^{t} \le d_{\text{E}.k}^{t-1} \\ \sum_{t=1}^{T} s_{\text{E}.k}^{t} \le S_{\text{E.max}} \\ \sum_{t=1}^{T} d_{\text{E}.k}^{t} \le D_{\text{E.max}} \end{cases} \tag{3}$$

where K is the total number of PEM electrolyzer units within the cluster, $k = 1,2,...,K$ u_{E}^{t}, s_{E}^{t}, and d_{E}^{t} are three binary variables respectively represent the on/off status, start-up action, and shut-down action of the PEM electrolyzer, α is the non-negligible heating time during the start-up phase of the electrolyzer the start-up delay, $S_{\text{E.max}}$ and $D_{\text{E.max}}$ respectively represents the maximum number of start-up and shut-down actions of the PEM electrolyzer within an operating cycle, $\mu_{\text{E.min}}$ and $\mu_{\text{E.max}}$ represent the minimum and maximum output percentages of the PEM electrolyzer, $\Delta P_{\text{E.max}}$ represents the full ramp-up power of the PEM electrolyzer, and λ_{E} represents the hydrogen production efficiency of the PEM electrolyzer.

In addressing the complexity of modeling multiple electrolyzer units, we adopt the CUC model to aggregate electrolyzer units into clusters, replacing numerous binary variables with a single integer variable for each cluster, simplifying the computation [34]. Thus, equation (3) can be replaced by equation (4) as below:

$$\begin{cases} \overline{s}_{\mathrm{E}}^{t-\alpha}-\overline{d}_{\mathrm{E}}^{t}=\overline{u}_{\mathrm{E}}^{t}-\overline{u}_{\mathrm{E}}^{t-1} \\ \overline{u}_{\mathrm{E}}^{1}=\overline{u}_{\mathrm{E}}^{T} \\ \overline{s}_{\mathrm{E}}^{t}\le K-\overline{s}_{\mathrm{E}}^{t-1} \\ \overline{d}_{\mathrm{E}}^{t}\le \overline{d}_{\mathrm{E}}^{t-1} \\ \sum_{t=1}^{T}\overline{s}_{\mathrm{E}}^{t}\le KS_{\mathrm{E.max}} \\ \sum_{t=1}^{T}\overline{d}_{\mathrm{E}}^{t}\le KD_{\mathrm{E.max}} \end{cases} \tag{4}$$

where $\overline{u}_{\mathrm{E}}^{t}$, $\overline{s}_{\mathrm{E}}^{t}$, and $\overline{d}_{\mathrm{E}}^{t}$ are three integer variables representing the number of on/off status, start-up action, and shut-down action of the clustered PEM electrolyzer, respectively.

2.3 Model of H_2 storage

H_2 storage can be regulated on both long-time scales (weeks) and short-time scales (hours) [30]. The hourly operating characteristics of H_2 storage can be determined as follows (weekly operational characteristics are almost the same) :

$$\begin{cases} SOH_{\mathrm{HT}}^{t+1}=SOH_{\mathrm{HT}}^{t}\left(1-\delta_{\mathrm{HT}}\right)+\dfrac{G_{\mathrm{HT.c}}^{t}\eta_{\mathrm{HT}}^{\mathrm{c}}\Delta t}{S_{\mathrm{HT}}},\text{charing} \\ SOH_{\mathrm{HT}}^{t+1}=SOH_{\mathrm{HT}}^{t}\left(1-\delta_{\mathrm{HT}}\right)-\dfrac{G_{\mathrm{HT.d}}^{t}\Delta t}{\eta_{\mathrm{HT}}^{\mathrm{d}}S_{\mathrm{HT}}},\text{discharing} \end{cases} \tag{5}$$

$$\begin{cases} 0\leqslant \eta_{\mathrm{HT}}^{\mathrm{c}}G_{\mathrm{HT.c}}^{t}\leqslant v_{\mathrm{HT.c}}^{t}S_{\mathrm{HT}} \\ 0\leqslant \eta_{\mathrm{HT}}^{\mathrm{d}}G_{\mathrm{HT.d}}^{t}\leqslant v_{\mathrm{HT.d}}^{t}S_{\mathrm{HT}} \end{cases} \tag{6}$$

$$v_{\mathrm{HT.c}}^{t}+v_{\mathrm{HT.d}}^{t}\le 1 \tag{7}$$

$$SOH_{\mathrm{HT}}^{0}=SOH_{\mathrm{HT}}^{T} \tag{8}$$

$$SOH_{\mathrm{HT}}^{\min}\leqslant SOH_{\mathrm{HT}}^{t}\leqslant SOH_{\mathrm{HT}}^{\max} \tag{9}$$

where SOH_{HT}^{t} represents the state of hydrogen (SOH) of the H_2 storage at the time $t(\forall t\in T)$, SOH_{HT}^{0} and SOH_{HT}^{T} are the capacity percentages of the H_2 storage at the beginning and end of the hydrogen charging and discharging sessions, respectively, $G_{\mathrm{HT.c}}^{t}$ and $G_{\mathrm{HT.d}}^{t}$ represent the volume of hydrogen charged and discharged at the time t, δ_{HT} represents the self-loss rate of the hydrogen storage, S_{HT} represents the installed capacity of the H_2 storage, $\eta_{\mathrm{HT}}^{\mathrm{c}}$ and $\eta_{\mathrm{HT}}^{\mathrm{d}}$ are the efficiencies of charging and discharging hydrogen in the storage tank, respectively, $v_{\mathrm{HT.c}}^{t}$ and $v_{\mathrm{HT.d}}^{t}$ are binary variables indicating the charging and discharging states of the storage tank, $SOH_{\mathrm{HT}}^{\min}$ and $SOH_{\mathrm{HT}}^{\max}$ represent the upper and lower limits of the storage tank capacity percentage, respectively.

For the transitions between weeks, the state at the final time of one week and the initial time of the following week must be the same. Continuity constraints can ensure a feasible transition between weeks [35]:

$$\begin{aligned} SOH_{\mathrm{HT}}^{w,t=1}&=SOH_{\mathrm{HT}}^{t=1} \\ SOH_{\mathrm{HT}}^{w,t=T}&=SOH_{\mathrm{HT}}^{t=T} \end{aligned} \tag{10}$$

where $SOH_{\mathrm{HT}}^{w,t}$ represents the SOH of the H_2 storage at the time t within the week $w(\forall w\in W)$.

2.4 Model of H_2-SF

H_2-SF is a continuous production equipment with operational flexibility [36]. The operating characteristics of H_2-SF can be determined as:

$$\left|D_{\mathrm{SF}}^{t}-D_{\mathrm{SF}}^{t-1}\right|\le \Delta D_{\mathrm{SF.max}}^{t} \tag{11}$$

$$D_{\mathrm{SF}}^{t}=G_{\mathrm{SF}}^{t}/\delta_{\mathrm{SF}} \tag{12}$$

$$\mu_{\mathrm{SF.min}}S_{\mathrm{SF}}\le D_{\mathrm{SF}}^{t}\le \mu_{\mathrm{SF.max}}S_{\mathrm{SF}} \tag{13}$$

where $\mu_{\mathrm{SF.min}}$ and $\mu_{\mathrm{SF.max}}$ represents the shaft furnace's minimum and maximum output percentages, respectively, $\Delta D_{\mathrm{SF.max}}^{t}$ is the full ramp-up power of the shaft furnace, δ_{SF} represents to the efficiency of the reduction process in the shaft furnace.

2.5 Model of HBI storage

The operational characteristics of HBI storage are similar to those of H_2 storage. However, due to the smaller capacity of HBI storage, it is scheduled on a daily cycle, stipulating that the storage capacity is restored to its initial state at the beginning and the end of each day. The operating characteristics of HBI Storage can be determined as follows:

$$\begin{cases} SOH_{\mathrm{HBI}}^{t+1}=SOH_{\mathrm{HBI}}^{t}\left(1-\delta_{\mathrm{HBI}}\right)+\dfrac{D_{\mathrm{HBI.c}}^{t}\eta_{\mathrm{HBI}}^{\mathrm{c}}\Delta t}{S_{\mathrm{HT}}},\text{charing} \\ SOH_{\mathrm{HBI}}^{t+1}=SOH_{\mathrm{HBI}}^{t}\left(1-\delta_{\mathrm{HBI}}\right)-\dfrac{D_{\mathrm{HBI.d}}^{t}\Delta t}{\eta_{\mathrm{HBI}}^{\mathrm{d}}S_{\mathrm{HBI}}},\text{discharing} \end{cases} \tag{14}$$

$$\begin{cases} 0\leqslant \eta_{\mathrm{HBI}}^{\mathrm{c}}D_{\mathrm{HBI.c}}^{t}\leqslant v_{\mathrm{HBI.c}}^{t}S_{\mathrm{HBI}} \\ 0\leqslant \eta_{\mathrm{HBI}}^{\mathrm{d}}D_{\mathrm{HBI.d}}^{t}\leqslant v_{\mathrm{HBI.d}}^{t}S_{\mathrm{HBI}} \end{cases} \tag{15}$$

$$v_{\mathrm{HBI.c}}^{t}+v_{\mathrm{HBI.d}}^{t}\le 1 \tag{16}$$

$$SOH_{\mathrm{HBI}}^{0}=SOH_{\mathrm{HBI}}^{T} \tag{17}$$

$$\begin{aligned} SOH_{\mathrm{HBI}}^{t}&=SOH_{\mathrm{HBI}}^{t+23} \\ t&=24(i-1)+1 \quad i=1,2,...,7 \end{aligned} \tag{18}$$

$$SOH_{\mathrm{HBI}}^{\min}\leqslant SOH_{\mathrm{HBI}}^{t}\leqslant SOH_{\mathrm{HBI}}^{\max} \tag{19}$$

where SOH_{HBI}^{t} represents the State of HBI (SOH) of the HBI storage at the time t, SOH_{HBI}^{0} and SOH_{HBI}^{T} represents the capacity percentages of the HBI storage at the beginning and end of the HBI charging and discharging sessions, respectively, $D_{\mathrm{HBI.c}}^{t}$ and $D_{\mathrm{HBI.d}}^{t}$ represents the mass of HBI charged and discharged at

the time t respectively, δ_{HBI} represents the self-loss rate of the HBI storage, S_{HBI} represents the installed capacity of the HBI storage, $\eta_{\mathrm{HBI}}^{\mathrm{c}}$ and $\eta_{\mathrm{HBI}}^{\mathrm{d}}$ are the efficiencies of charging and discharging HBI in the storage, respectively, $v_{\mathrm{HBI.c}}^{t}$ and $v_{\mathrm{HBI.d}}^{t}$ are binary variables indicating the charging and discharging states of the HBI storage, $SOH_{\mathrm{HBI}}^{\min}$ and $SOH_{\mathrm{HBI}}^{\max}$ represents the upper and lower limits of the HBI storage capacity percentage, respectively.

2.6 Model of EAF

EAF is a continuous production equipment that generally operates at its rated power. It also has a certain degree of operational flexibility. The operating characteristics of the electric arc furnace are described as:

$$\mu_{\mathrm{EAF.min}} S_{\mathrm{EAF}} \le D_{\mathrm{EAF}}^{t} \le \mu_{\mathrm{EAF.max}} S_{\mathrm{EAF}} \tag{20}$$

$$\left| D_{\mathrm{EAF}}^{t} - D_{\mathrm{EAF}}^{t-1} \right| \le \Delta D_{\mathrm{EAF.max}}^{t} \tag{21}$$

$$S_{\mathrm{EAF}}^{t} = D_{\mathrm{EAF}}^{t} / \gamma_{\mathrm{EAF}} \tag{22}$$

where $\mu_{\mathrm{EAF.min}}$ and $\mu_{\mathrm{EAF.max}}$ represent the EAF's minimum and maximum output percentages, respectively, $\Delta D_{\mathrm{EAF.max}}^{t}$ represents the full ramp-up power of the electric arc furnace, γ_{EAF} corresponds to the efficiency of steelmaking in the electric arc furnace.

3. METHODOLOGY

3.1 Description of the multi-period optimization model of HBSS

3.1.1 Assumptions

The following assumptions are made for the problem of multi-period optimization problems of HBSS setups:

- Each machine is constrained in capacity.
- There are no times for transportation of the products.
- Shortages are not permitted.
- There are no costs for shadow products.

3.1.2 Objective function

The objective function is to minimize the LCOS across the lifecycle (n years) of the system. The lifecycle is divided into N periods, and the multi-period sequence S is denoted as:

$$S = \left[S_1, S_2, \cdots, S_i, \cdots, S_N \right] \tag{23}$$

where S_i represents the i th period, where $i = 1, 2, \cdots, N$.

The present value factor is denoted as:

$$R^k = (1+r)^{-k} \tag{24}$$

where k is the number of years from when the cost occurs to the beginning of the planning period; R^k is the present value factor for the k th year; r is the discount rate. The objective function can be described as:

$$\mathrm{LCOS} = \frac{\sum_{i=1}^{N} R^{s_i} C_{\mathrm{inv}}^{i} - R^{n} F_{\mathrm{R}} + \sum_{k=1}^{n} R^{k} C_{\mathrm{ope}}^{k}}{TSP}$$
$$C_{\mathrm{ope}}^{k} = C_{\mathrm{mai}}^{k} + C_{\mathrm{raw}}^{k} + C_{\mathrm{grid}}^{k} + C_{\mathrm{lab}}^{k} + C_{\mathrm{emi}}^{k} \tag{25}$$

where C_{inv}^{i} represents the investment cost for the starting year of S_i, C_{ope}^{k} represents the operational cost in the k th year, C_{mai}^{k}, C_{raw}^{k}, C_{grid}^{k}, C_{lab}^{k}, and C_{emi}^{k} represents capital, maintenance, raw material, power purchase, labor, and emission costs in the k th year, respectively. R^n is the present value factor at the end of the planning period. F_{R} represents the residual value of the equipment at the end of the planning period, as shown in formula (25):

$$F_{\mathrm{RV}} = \sum_{i=1}^{S_N} \sum_{j=1}^{M} \left(C_{\mathrm{inv}}^{i,j} - C_{\mathrm{dep}}^{i,j} \right) \tag{26}$$

where M is the total type amount of equipment. $C_{\mathrm{inv}}^{i,j}$ and $C_{\mathrm{dep}}^{i,j}$ are the investment cost and depreciation expense of equipment type j within the i th period respectively.

3.1.3 Constraints

HBSS is designed to satisfy the hourly steel demand, so balances on electricity, hydrogen, DRI/HBI, and steel demands are considered when scheduling HBSS operations. The energy balance constraints are described as shown in formula (26):

$$\begin{cases} P_{\mathrm{WT}}^{t} + P_{\mathrm{PV}}^{t} + P_{\mathrm{G}}^{t} = P_{\mathrm{E}}^{t} + P_{\mathrm{SF}}^{t} + P_{\mathrm{EAF}}^{t} \\ G_{\mathrm{E}}^{t} + G_{\mathrm{HT.d}}^{t} = G_{\mathrm{HT.c}}^{t} + G_{\mathrm{SF}}^{t} \\ D_{\mathrm{SF}}^{t} + D_{\mathrm{HBI.d}}^{t} = D_{\mathrm{HBI.d}}^{t} + D_{\mathrm{EAF}}^{t} \\ S_{\mathrm{EAF}}^{t} = S_{\mathrm{N}}^{t} \end{cases} \tag{27}$$

where P_{WT}^{t} and P_{PV}^{t} represent the power from wind and photovoltaic sources at the time t, respectively, S_{N}^{t} denotes the hourly rated crude steel load demand of the HBSS system.

The constraint of renewable energy penetration rate should also be considered, as shown in formula (27):

$$\omega = \sum_{t=1}^{8760} (P_{\mathrm{WT}}^{t} + P_{\mathrm{PV}}^{t}) / \sum_{t=1}^{8760} (P_{\mathrm{WT}}^{t} + P_{\mathrm{PV}}^{t} + P_{\mathrm{grid}}^{t}) \tag{28}$$

where $t = 1, 2, \cdots, 8760$.

3.2 Solving the multi-period problem with rolling-horizon

Based on the multi-period optimization model described above, the underlying time structure can be decomposed into multiple coupled optimization problems $\{P_0,\ldots,P_T\}$ [33], which can be defined below:

$$\begin{aligned} \min \quad & f_t(x_t) \\ \text{s.t.} \quad & g_t(\xi_t, x_t, \vartheta_t) \le 0 \\ & (\xi_t, x_t, \vartheta_t) \in \Xi_t \times X_t \times \Theta_t \end{aligned} \tag{29}$$

Each optimization problem belongs to a time period $t \in [T] := \{0,\ldots,T\}$, where $T \in \mathbb{N}_0$. Each time period t, P_t has a set of variables ξ_t with start state variables defined on a domain Ξ_t and end-state variables ϑ_t defined on a domain Θ_t. Interior variables x_t are neither start-state nor end-state variables and are defined on a domain X_t. The start-state variables ξ_t and the end-state variables ϑ_t connect the current time period and the previous or subsequent time period, respectively. We assume that the end-state set of the current time period is contained in the start-state set of the subsequent period.

We further define the multi-period problem $P_{t,\mu}$ for $\mu \in \mathbb{N}_0$, $\mu + t \le T$, starting at period t as

$$\begin{aligned} \min \quad & \sum_{j=t}^{t+\mu} f_j(x_j) \\ \text{s.t.} \quad & g_j(\xi_j, x_j, \vartheta_j) \le 0 && \forall j \in \{t,\ldots,t+\mu\} \\ & \xi_j = \vartheta_{j-1} && \forall j \in \{t+1,\ldots,t+\mu\} \\ & (\xi_j, x_j, \vartheta_j) \in \Xi_j \times X_j \times \Theta_j && \forall j \in \{t,\ldots,t+\mu\} \end{aligned} \tag{30}$$

The index μ can be suppressed if it is 0.

The schematic depiction of the rolling horizon approach is shown in Fig.3.

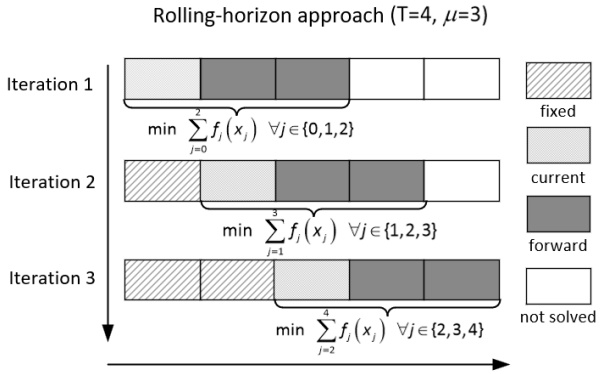

Fig.3. Schematic depiction of the rolling horizon approach

The multi-period optimization model spans a time frame from 2025 to 2050. Employing the rolling-horizon approach, the underlying optimization problem is repeatedly modeled every five years, then solved, and then shifted forward by five years, while all variables slipping out of the decision horizon are considered fixed in subsequent iterations until the entire time horizon is passed through.

4. RESULTS AND DISCUSSION

4.1 Input data

Capital and operational costs for the main equipment [24] are shown in Table 1 and Table 2. K-means clustering algorithm was employed to cluster typical weekly wind and solar resources under each seasonal type (winter, summer, and other seasons). The generated values over a week in the three seasons are shown in Fig.4. The ToU electricity prices for summer, winter, and other seasons of the Jiangxi Province are shown in Fig. 5.

Table.1

Parameters of capital cost.

Capital expenditure (CAPEX) in USD					
Component	Period Start				
	2025	2030	2035	2040	2045
WT/kW	1594	1497	1401	1242	1083
PV/kW	1091	957	823	646	468
PEM/kW	1432	1142	852	646	441
PEM efficiency/ kWh/kg	57.5	55.5	53.8	52.1	50.5
Scrap ratio/%	20	30	40	50	60
H_2 Storage/kWh	18				
EAF/t per annum	285				
H_2-SF/t per annum	355				

Table.2

Parameters of operating cost.

Operational expenditure (OPEX) in USD	
Renewable energy penetration	90%
demand for steel	8760 tonnes/ annum (1 tonne/hour)
PEM Fixed OPEX	3% of CAPEX/ annum
H_2-SF Fixed OPEX	
EAF Fixed OPEX	
H_2 Storage Fixed OPEX	1% of CAPEX/ annum
HBI storage Fixed OPEX	
WT Fixed OPEX	28/kW/ annum
PV Fixed OPEX	19/kW/ annum
Labor	38.4/ tonne crude steel
Emission price	50/ tCO_2
Raw material for steelmaking	51/ tonne crude steel
Iron ore (DR-grade pellets)	152/ tonne DRI
Scrap iron	400/ tonne crude steel
Direct emission factor from EAF	73 kgC02/ tonne crude steel
Indirect emission factor from DRI	56 kgC02/ tonne crude steel
Grid emission factor	0.5703/ tCO_2/kWh

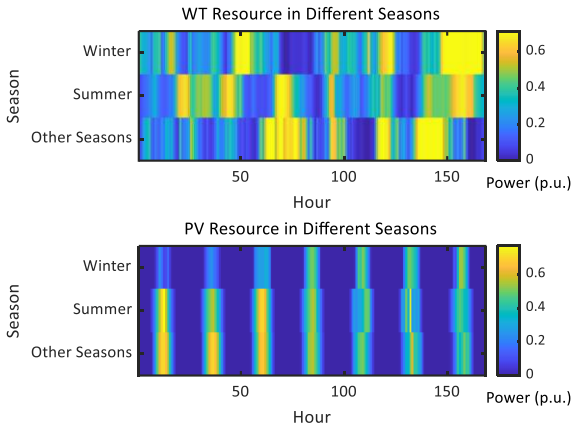

Fig.4. WT and PV resource in different seasons

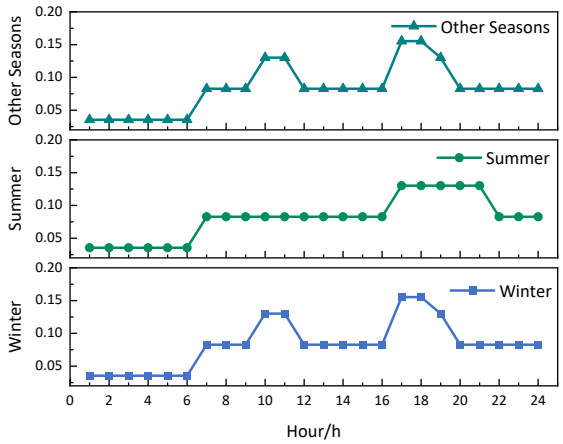

Fig.5. ToU electricity pricing for different seasons

All the computations were tested on a desktop computer with a CPU (2.50GHz) and 16.0GB RAM.

4.2 Results and analysis

The weekly and hourly resolutions of H_2 storage and HBI storage are shown in Fig.6. The weekly resolution is observed within a typical winter week.

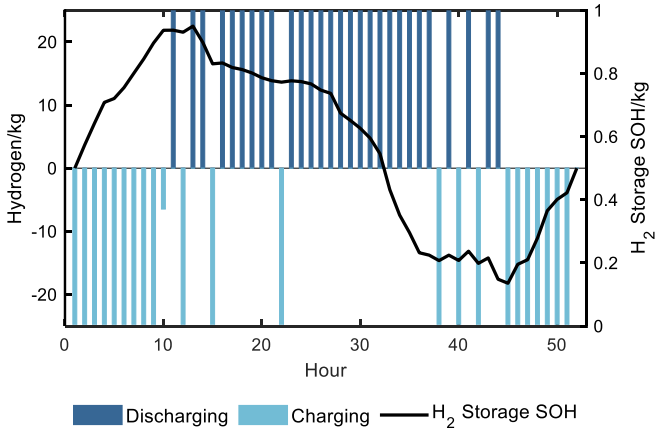

(a) Weekly operational profile of H2 storage

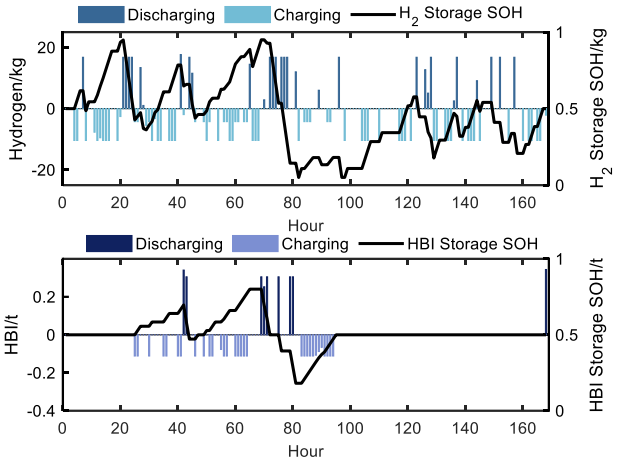

(b) Hourly operational profile of H_2 and HBI storage

Fig.6. Operation profile of H_2 and HBI storage

The regulatory functions of these two energy storage technologies are markedly different, primarily because of their varying adjustment time. Specifically, H_2 storage modulates hydrogen production continuously throughout each week and hour. This adjustment maintains a balanced supply-demand equation for the H_2-SF. On the other hand, HBI storage is strategically employed to ensure a consistent and reliable DRI supply for the EAF, thereby facilitating a stable and uninterrupted load supply.

We conducted comparative experiments to compare the advantages of the rolling-horizon approach with the single-period approach and the forward-looking approach. The optimal result of LCOS and investment strategy of different equipment applied to different approaches are shown in Fig.7 and Fig.8.

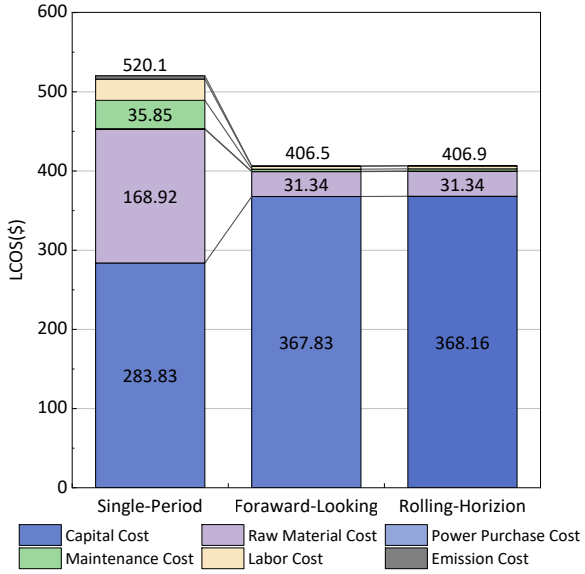

Fig.7. Optimal result of LCOS for different approaches applied to multi-period problems

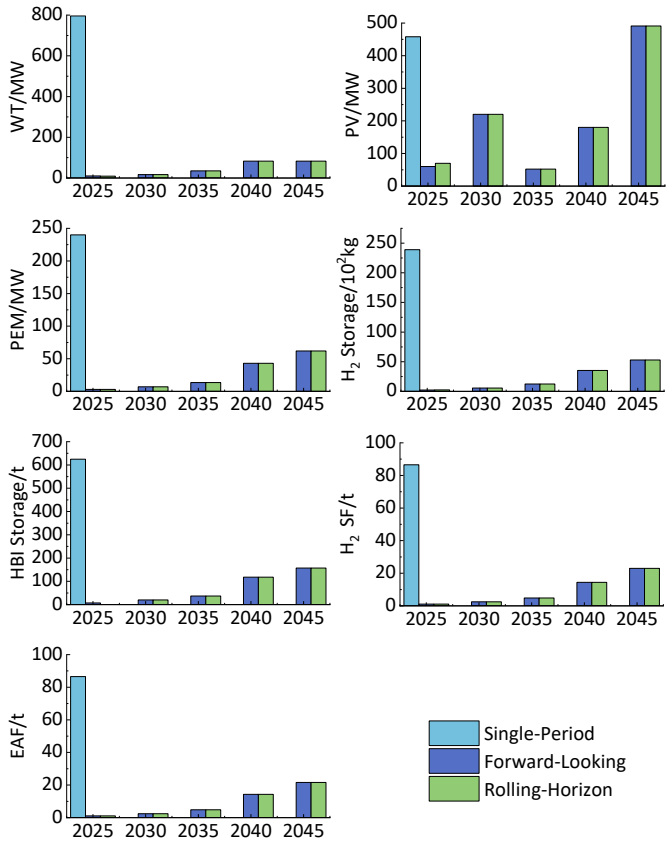

Fig.8. Optimal investment results for different approaches applied to the multi-period problem

It can be observed that the LCOS obtained from the forward-looking approach and the rolling-horizon approach are \$406.5 and \$406.9, differing by only 0.1%. In contrast, the LCOS obtained from the single-period approach is \$520, significantly higher than the other two. Because the single-period approach does not consider the changing parameters within the future forecast horizon, leading to decisions that are not adaptable to the system's operational state over long periods.

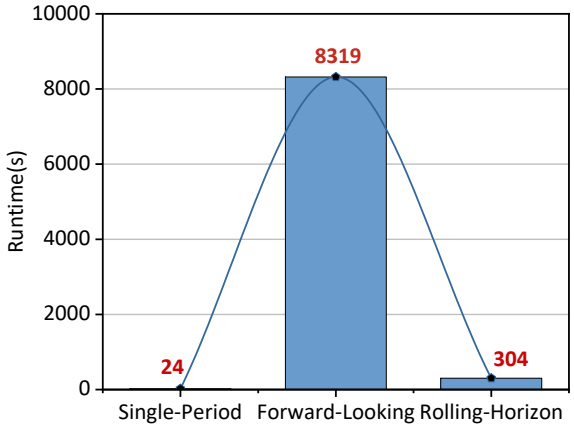

Fig.9. Runtime for different solution approaches applied to the multi-period problem

Regarding computational efficiency, as shown in Fig.9, the runtime for the forward-looking approach is the longest. In contrast, the single-period approach has the shortest runtime but the worst economic-friendly solution. Using the sequential decision solved by the rolling-horizon approach, we can obtain a similar investment decision as the forward-looking approach in a more optimistic computational time.

CONCLUSIONS

Multi-stage optimization models can consider the impact of future decision periods, which aims to enhance the system's economic and environmental potential for a long time. This paper provided a multi-period optimization model for HBSS. It employed the rolling-horizon approach to exploit the multi-period optimization problem into sequences of coupled optimization problems, which delivers provable near-optimal solutions and significantly improves computational efficiency compared to the forward-looking approach.

In addition, forward parameters must be considered as uncertain in application settings. The rolling-horizon approach can adapt to future parameter changes by making periodic decisions. Hence, further research on this topic commits to considering uncertainty in application. As for our future work, it is of interest to research how the rolling-horizon approach can be extended so that it can hedge against uncertainties.

DECLARATION OF INTEREST STATEMENT

The authors declare that they have no known competing financial interests or personal relationships that could have appeared to influence the work reported in this paper. All authors read and approved the final manuscript.

ACKNOWLEDGEMENT

This work was supported in part by the National Nature Science Foundation of China (52207112, 51977005) and National Key Research and Development Program of China (2022YFB2403402).

REFERENCE

[1] Yan R, Wang J, Wang J, Tian L, Tang S. A two-stage stochastic-robust optimization for a hybrid renewable energy CCHP system considering multiple scenario-interval uncertainties. Energy 2022;247:123498.

[2] Lee C-C, Hussain J, Chen Y. The optimal behavior of renewable energy resources and government's energy consumption subsidy design from the perspective of

green technology implementation. Renew Energy 2022;195:670–80.
[3] Wang C, Walsh SD, Weng Z, Haynes MW, Summerfield D, Feitz AJ. Green steel: Synergies between the Australian iron ore industry and the production of green hydrogen. 2023.
[4] Lei T et al. Global iron and steel plant CO2 emissions and carbon-neutrality pathways. 2023;1–7.
[5] Tang J, Chu M, Li F, Feng C, Liu Z, Zhou Y. Development and progress on hydrogen metallurgy. Int J Miner Metall Mater 2020;27(6):713–23.
[6] Ranzani da Costa A, Wagner D, Patisson F. Modelling a new, low CO2 emissions, hydrogen steelmaking process. J Clean Prod 2013;46:27–35.
[7] Sarker AK, Azad AK, Rasul MG, Doppalapudi AT. Prospect of Green Hydrogen Generation from Hybrid Renewable Energy Sources: A Review. 2023;16(3):1556.
[8] Fang YR et al. Neutralizing China's transportation sector requires combined decarbonization efforts from power and hydrogen supply. Appl Energy 2023;349:121636.
[9] Hermesmann M, Tsiklios C, Müller TE. The environmental impact of renewable hydrogen supply chains: Local vs. remote production and long-distance hydrogen transport. Appl Energy 2023;351:121920.
[10] Gajdzik B, Wolniak R, Grebski WW. An econometric model of the operation of the steel industry in Poland in the context of process heat and energy consumption. 2022;15(21):7909.
[11] Duarte P. Trends in H2-based steelmaking. 2019;43(1):27–32.
[12] Sustainability | Free Full-Text | The Direct Reduction of Iron Ore with Hydrogen. Accessed: Dec. 11, 2023. [Online]. Available: https://www.mdpi.com/2071-1050/13/16/8866
[13] Li F et al. Quantifying the energy saving potential and environmental benefit of hydrogen-based steelmaking process: Status and future prospect. Appl Therm Eng 2022;211:118489.
[14] Karakaya E, Nuur C, Assbring L. Potential transitions in the iron and steel industry in Sweden: Towards a hydrogen-based future? J Clean Prod 2018;195:651–63.
[15] Öhman A, Karakaya E, Urban F. Enabling the transition to a fossil-free steel sector: The conditions for technology transfer for hydrogen-based steelmaking in Europe. Energy Res Soc Sci 2022;84:102384.
[16] Zhang S, Chen WN. Assessing the energy transition in China towards carbon neutrality with a probabilistic framework. 2022;13(1):87.
[17] Atsushi M, Uemura H, Sakaguchi TKTR. MIDREX processes. 2010;29(8).
[18] Watakabe S et al. Operation Trial of Hydrogenous Gas Injection of COURSE50 Project at an Experimental Blast Furnace. 2013;53:2065–71.
[19] Deerberg G, Oles M, Schlögl RCI. The Project Carbon2Chem®. 2018;90(10):1365–68.
[20] Xylia M, Silveira S, Duerinck J, Meinke-Hubeny FE. Weighing regional scrap availability in global pathways for steel production processes. 2018;11:1135–59.
[21] Gusev AL et al. Production of hydrogen and carbon in the petrochemical industry by cracking of hydrocarbons in the process of heat utilization in steel production. Int J Hydrog Energy 2023;48(40):14954–63.
[22] Liu W, Zuo H, Wang J, Xue Q, Ren B, Yang F. The production and application of hydrogen in steel industry. Int J Hydrog Energy 2021;46(17):10548–69.
[23] Toktarova A, Göransson L, Johnsson F. Design of Clean Steel Production with Hydrogen: Impact of Electricity System Composition. Energies 2021;14(24).
[24] Bhaskar A, Abhishek R, Assadi M, Somehesaraei HN. Decarbonizing primary steel production: Techno-economic assessment of a hydrogen based green steel production plant in Norway. J Clean Prod 2022;350:131339.
[25] Astier J, Krug JC, de Pressigny YdL. Technico-economic potentialities of hydrogen utilization for steel production. Int J Hydrog Energy 1982;7(8):671–79.
[26] Shahabuddin M, Brooks G, Rhamdhani MA. Decarbonisation and hydrogen integration of steel industries: Recent development, challenges and technoeconomic analysis. J Clean Prod 2023;395:136391.
[27] Bhaskar A, Assadi M, Somehsaraei HN. Decarbonization of the Iron and Steel Industry with Direct Reduction of Iron Ore with Green Hydrogen. Energies 2020;13(3).
[28] Griffiths S, Sovacool BK, Kim J, Bazilian M, Uratani JM. Industrial decarbonization via hydrogen: A critical and systematic review of developments, socio-technical systems and policy options. Energy Res Soc Sci 2021;80:102208.
[29] Gielen D, Saygin D, Taibi E, Birat J-P. Renewables-based decarbonization and relocation of iron and steel making: A case study. J Ind Ecol 2020;24(5):1113–25.
[30] Shang J, Gao J, Jiang X, Liu M, Liu D. Optimal configuration of hybrid energy systems considering power to hydrogen and electricity-price prediction: A two-stage multi-objective bi-level framework. 2023;263:126023.
[31] Bohlayer M, Bürger A, Fleschutz M, Braun M, Zöttl G. Multi-period investment pathways - Modeling

approaches to design distributed energy systems under uncertainty. Appl Energy 2021;285:116368.
[32] Pecenak ZK, Stadler M, Fahy K. Efficient multi-year economic energy planning in microgrids. Appl Energy 2019;255:113771.
[33] Glomb L, Liers F, Rösel F. A rolling-horizon approach for multi-period optimization. Eur J Oper Res 2022;300(1):189–206.
[34] Palmintier BS, Webster MD. Heterogeneous Unit Clustering for Efficient Operational Flexibility Modeling. IEEE Trans Power Syst 2014;29(3):1089–98.
[35] Sánchez A, Martín M, Zhang Q. Optimal design of sustainable power-to-fuels supply chains for seasonal energy storage. Energy 2021;234:121300.
[36] Anameric B, Kawatra SK. Properties and features of direct reduced iron. 2007;28(1):59–116.